JOURNAL OF GEOPHYSICAL RESEARCH, VOL. 102, NO. E8, PAGES 19,293–19,306, AUGUST 25, 1997

# Raman spectroscopy for mineral identification and quantification for in situ planetary surface analysis: A point count method

Larry A. Haskin, Alian Wang, Kaylynn M. Rockow, Bradley L. Jolliff, Randy L. Korotev, and Karen M. Viskupic

Department of Earth and Planetary Sciences and McDonnell Center for the Space Sciences
Washington University, St. Louis, Missouri

**Abstract.** Quantification of mineral proportions in rocks and soils by Raman spectroscopy on a planetary surface is best done by taking many narrow-beam spectra from different locations on the rock or soil, with each spectrum yielding peaks from only one or two minerals. The proportion of each mineral in the rock or soil can then be determined from the fraction of the spectra that contain its peaks, in analogy with the standard petrographic technique of point counting. The method can also be used for nondestructive laboratory characterization of rock samples. Although Raman peaks for different minerals seldom overlap each other, it is impractical to obtain proportions of constituent minerals by Raman spectroscopy through analysis of peak intensities in a spectrum obtained by broad-beam sensing of a representative area of the target material. That is because the Raman signal strength produced by a mineral in a rock or soil is not related in a simple way through the Raman scattering cross section of that mineral to its proportion in the rock, and the signal-to-noise ratio of a Raman spectrum is poor when a sample is stimulated by a low-power laser beam of broad diameter. Results obtained by the Raman point-count method are demonstrated for a lunar thin section (14161,7062) and a rock fragment (15273,7039). Major minerals (plagioclase and pyroxene), minor minerals (cristobalite and K-feldspar), and accessory minerals (whitlockite, apatite, and baddeleyite) were easily identified. Identification of the rock types, KREEP basalt or melt rock, from the 100-location spectra was straightforward.

## 1. Introduction

Whatever aspect of a solid planetary body may be of interest, whether it is origin and geological evolution of the object, resources, exobiology, hydrology, atmosphere, or something else, knowledge of the principal materials present at the surface of the body will be essential to proper understanding and interpretation. Chemical and mineral compositions of surface materials are such fundamental properties that any exploratory mission can be regarded as successful to a substantial extent if they have been definitively characterized [e.g., *Meyer et al.*, 1996].

For any rock or soil on a planetary surface, we wish to determine the identity of each component mineral, the end-member composition of each mineral, and the fraction of the rock or soil

$Mg^{2+}/Fe^{2+}$ ratios of pyroxenes. We also indicated that small and robust Raman spectrometers could be developed for remote sensing on a planetary surface [see also *Wdowiak et al.*, 1995; *Dyar et al.*, 1996; *Kerridge et al.*, 1996]. The main purpose of the work described here is to show how best to quantify the relative abundances of minerals in a rock or soil using laser Raman spectroscopy. We also show how information can be obtained on grain size, mineral association, and rock texture. The same procedures can be used for nondestructive, first-order mineralogical characterization of samples in the laboratory that would otherwise require thin sections to be prepared.

We might wish that the relative Raman peak intensities of each mineral in the spectrum of a polyphase target could be related in a straightforward way to the fraction of that mineral

roxene grains are zoned, ranging in Mg' (mole percent $Mg^{2+}/[Mg^{2+} + Fe^{2+}]$) from 82 to 5 and in Wo content from 3 to 32 mol %.

For this first experiment, a grid was overlain on a reflected-light photomicrograph of the thin section. Each grid location was located visually on the thin section, centered under the laser beam by adjusting the mechanical stage of the Raman microprobe, and analyzed. The equally spaced grid locations were ~220 μm apart. Their positions on the arbitrarily preselected grid were strictly adhered to, and no adjustment was made even where the beam impinged on a grain boundary, crack, pit, or other inconvenient location. The microscope stage was adjusted vertically as needed, however, to ensure that the top of the thin section was in laser focus, to accommodate the depth of field of the laboratory instrument.

### 2.2. Rock Fragment 15273,7039

To test more realistically the ability of Raman spectroscopy to identify minerals in a rock on a planetary surface, we analyzed the surface of a small lunar rock fragment. The only preparation the surface received was an ultrasonic rinse with acetone. The sample, 15273,7039, was a previously unstudied, 32-mg fragment from regolith sample 15270, which was collected at station 6 on the Apennine Front during the Apollo 15 mission. We selected it because under the binocular microscope it appeared to be a fine-grained igneous rock with a basaltic texture. For Raman analysis, it rested in a shallow well (~0.5 cm × 2 mm deep) drilled into an aluminum block. The block was then taped to a glass slide and placed on the microscope stage of the laser Raman system. The block was moved in fixed increments of distance (~330 μm) along the $X$ axis until the width of the sample had been traversed, then it was moved by one increment in the $Y$ direction and the next line of grid locations was traversed. We adhered strictly to these increments regardless of the image seen in the microscope. The rock surface analyzed was only roughly parallel to the plane of the microscope stage. The microscope was brought into rough focus at each location. (This is an advantage not anticipated for a planetary spectrometer, which will have to make do with a lower power objective that has a greater effective depth of field. Preliminary experiments with such a low power objective indicate that the mineral grains can be significantly out of optical focus and still yield adequate spectra [*Wang et al.*, 1997a].)

### 2.3. Mineral Identification

After the spectra of the 100 grid locations had been taken on thin section 14161,7062, further Raman analyses were done on selected spots to aid in mineral identification. For the same purpose, following Raman analysis of 15273,7039, we prepared a polished section of the rock fragment, thick enough to avoid any laser beam interaction with the epoxy bonding resin. Standard petrographic analysis confirmed our mineral identifications based on the Raman analysis. The sample turned out to be a KREEP basalt, and not a mare basalt, both of which occur in regolith sample 15270 [*Korotev*, 1987].

### 2.4. Effects of Crystal Orientation

For later examination of the effects of crystal orientation on Raman intensities of specific vibrational modes, several targeted mineral grains in the thin section of 14161,7062 and the polished section of 15273,7039 were centered on the microscope stage of the Raman microprobe system. The incident laser beam is linearly polarized, with its electric vector ($\vec{E}$) parallel to the $X$ axis of the microscope stage. Mineral grains with subhedral to euhedral crystal shapes were chosen, in order to align an edge or a cleavage of each grain with $\vec{E}$. After each spectrum was taken, the microscope stage (as well as the target mineral grain) was rotated relative to $\vec{E}$. A spectrum was recorded after each 30° or 45° rotation. In these measurements, the rotational axis of the microscope stage was not necessarily aligned along a true crystallographic axis of the studied grains. These orientation tests thus do not constitute a complete measurement of polarization spectra, but they demonstrate clearly the large changes in relative peak intensity likely to be encountered in spectra obtained by point counting.

## 3. Results and Discussion

### 3.1. Point Counts

The results obtained for the grid locations are summarized in Tables 1 and 2. For each sample, the locations are numbered in the order in which their spectra were taken, and location numbers are listed for each mineral. Identifications are listed as either "single," if the spectrum was dominated by peaks of a single mineral, or "mixed," if peaks of more than one mineral could be identified in the spectrum. For mixed spectra, half an occurrence was assigned to each of the two minerals identified in the spectrum, regardless of the relative intensities of the peaks from each mineral. (Only two locations with peaks from three minerals were encountered, in rock fragment 15273,7039.)

**3.1.1. Thin section 14161,7062.** Figure 1a is a photomicrograph of thin section 14161,7062. Figure 1b shows an outline of grain boundaries and the results of the 100-point grid of Raman analyses. Figure 2 shows typical examples of spectra obtained on the 100-point grid. Out of 100 grid locations, 91 mineral identifications were made from 89 spectra (Table 1). One interesting spectrum (location 2) turned out to be that of the mineral baddeleyite ($ZrO_2$), found as a tiny crystal embedded beneath the surface of the thin section in a region of mesostasis. This and other accessory minerals were found by Raman analysis among the 100 locations in both the thin section and in the rock fragment. Of the 11 grid locations that yielded no mineral identifications, three (28, 45, 46) were voids. Seven locations gave no informative spectra. At three of these seven locations (23, 79, 93), the laser encountered only the epoxy resin that was used to glue the parent rock to its supporting glass slide and which impregnates fractures and voids in the rock. At the other four of these locations (3, 12, 21, 80) the spectra had high backgrounds from fluorescence that overwhelmed any signal that may have been present from a mineral. It appears that the fusion of epoxy resin under the laser caused this type of fluorescence. The epoxy resin has a high Raman sensitivity (cross section). We obtained substantial peaks from epoxy resin in nearly all spectra (Figure 2), indicating that Raman scattering is observed from epoxy occurring beneath the 30 μm thickness of rock of a standard petrographic thin section. This demonstrates that the sampling depth exceeds 30 μm and that useful mineral identifications could be made on rocks with thin surface coatings [*Israel et al.*, 1996; 1997]. At the last of the 11 locations (29), which was taken in an area of mesostasis, the spectrum did not contain any sharp peaks such as those characteristic of silicate or phosphate minerals. Instead, it contained rather broad bands that resemble those of the spectrum for hematite, but an $Fe^{3+}$ mineral is not reasonable for

**Table 1.** Results of Modal Analyses of Thin Section 14161,7062

| | Standard Analysis | | Raman Analysis | | | | |
|---|---|---|---|---|---|---|---|
| | Whole TS, % | 100-pt Grid, % | 100-pt Grid, % | Single (*N*) | Mixed (*N*) | Point Number | |
| | | | | | | Single | Mixed |
| Plagioclase | 57 | 58.5 | 56.5 | 56 | 1 | 6, 9, 11, 14-17, 20, 22, 26, 27, 30, 31, 34, 36, 38-41, 44, 47-54, 57-59, 62-65, 67, 68, 70, 71, 74-76, 81, 82, 86-89, 92, 94-100 | 32 |
| Orthopyroxene | 10 | 8 | 12 | 12 | | 4, 5, 10, 13, 24, 25, 35, 37, 61, 83-85 | |
| Clinopyroxene | 21 | 16.5 | 11 | 10 | 2 | 1, 7, 18, 19, 55, 66, 69, 72, 73, 78 | 32, 60 |
| K-feldspar | 0.8 | 2 | 7.5 | 7 | 1 | 8, 42, 43, 56, 77, 90, 91 | 60 |
| Whitlockite | 0.3 | | 1 | 1 | | 33 | |
| Mesostasis* | 5 | 11 | | | | | |
| Ilmenite | 5 | | | | | | |
| Baddeleyite | | | 1 | 1 | | 2 | |
| Zircon | 1 | | | | | | |
| Unidentified | | | 1 | 1 | | 29 | |
| Fluorescence* | | | 4 | 4 | | 3, 12, 21, 80 | |
| Epoxy resin | | | 3 | 3 | | 23, 79, 93 | |
| Void | | 4 | 3 | 3 | | 28, 45, 46 | |
| Total | 100 | 100 | 100 | 98 | 4 | | |

The percentage of each mineral in the whole thin section (TS) is given based on modal analysis (2057 points) done with a petrographic microscope. In this analysis, voids in the thin section were not counted. The percentages obtained for the 100 grid points by standard modal analysis (supplemented with backscattered electron images from the electron microprobe in ambiguous cases) and by the Raman spectroscopic technique are listed; four points were voids. The number of occurrences is given of each mineral obtained by the Raman technique. For a few points ("mixed"), the spectra indicated the presence of two minerals; in these cases, ½ of an occurrence was assigned to each mineral for the purpose of computing the percentages for Raman analysis of 100-point grid.

*Mesostasis represents areas between grains of the major minerals that containing accessory minerals too small to be identified petrographically. From four locations, a strong fluorescence signal was obtained, obscuring any signal that may have been present from a mineral.

a lunar rock. We suspect the phase giving rise to this spectrum is an oxide. It is conceivable that concentrating the 5 mW laser beam on a ~1 μm spot on the sample in air caused oxidization of some $Fe^{2+}$-bearing nonsilicate mineral. We have not observed thermal alteration to be a general problem with most materials we have analyzed. The lower power density (larger spot size) we anticipate using for on-surface planetary work and a less oxidizing planetary atmosphere will reduce this problem.

In Table 1, the relative abundances of the minerals as determined from the Raman experiment (Raman Analysis, 100-pt Grid) are compared to those determined by petrographic examination of the same grid locations (Standard Analysis, 100-pt Grid). As the grid locations are the same for both the Raman spectroscopic analysis and the petrographic analysis, we might expect virtually identical results from both procedures. For the major minerals, the results are similar but not identical. Differences occur mainly because the Raman experiment samples a volume beneath the surface that is seen petrographically and because the Raman cross sections for all minerals are not equal but favor observation of some minerals over others. The Raman experiment found slightly less plagioclase (56.5%) than the petrographic analysis of the same grid locations (58.5%). Four locations identified petrographically as plagioclase were not identified as such by their Raman spectra. Two of the spectra from these locations (3, 12) were strongly fluorescent, another (8) was identified as a K-feldspar, and the fourth (85) was identified as an orthopyroxene. All of these grid locations were at or near grain contacts. Either the Raman location and the petrographic identifications were made on opposite sides of the boundaries or the Raman instrument recorded the mineral that lay along a sloping contact just beneath a shallow, surface plagioclase grain. This can occur because the Raman scattering cross section for plagioclase is lower than those for pyroxenes, olivine, and many minor and accessory minerals, so a weak signal from a thin surface layer of plagioclase can be overwhelmed by the signal from a stronger Raman scatterer beneath it.

There is also good agreement between the two methods for total pyroxene (23% compared with 24.5%), although the distribution between orthopyroxene and clinopyroxene differs (Table 1). Strong compositional zoning from orthopyroxene to pigeonite to Fe-augite occurs in this sample over distances of a few micrometers, and in some cases, the exact location of the transition from orthopyroxene to clinopyroxene by the petrographic method could be determined only approximately. Also, a few pyroxene spectra were ambiguous with respect to classification as orthopyroxene versus clinopyroxene because they showed characteristics of both.

The results of the two techniques appear to be drastically different for K-feldspar and mesostasis; this results because, in most cases where a grid location fell within mesostasis, we could not distinguish petrographically among the different mesostasis minerals. At only two such locations were K-feldspar grains coarse enough to identify optically, but K-feldspar peaks were identified in the spectra of eight mesostasis locations by the Raman technique (Table 1). Mesostasis is a mineralogically complex, fine-grained product of rapid crystallization of residual liquid, and it contains a variety of accessory minerals. K-feldspar is a principal mineral in the mesostasis, but ilmenite, pyroxferroite, baddeleyite, zircon, and whitlockite are also observed in high-magnification backscattered-electron images. It was impos-

**Table 2.** Results of Modal Analyses of KREEP Basalt Rocklet 15273,7039

| | TS, % | Raman, % | Single (N) | Mixed (N) | Point Number: Single | Point Number: Mixed | Percent Occurring With: Alone | Plag | Opx | Cpx | Ksp | Cr | Phos |
|---|---|---|---|---|---|---|---|---|---|---|---|---|---|
| | | | | | 2, 6, 11, 13, 15, 19, 22, 23, 26, 32, | 4, 8, 12, 14, 29, 40, 42, 44, 46, 47, | | | | | | | |
| Plagioclase | 50.0 | 42 | 29 | 26 | 33, 38, 39, 43, 48, 49, 52, 53, 56, 57, 60, 63, 73, 75, 79, 89, 92, 98, 99 | 50, 59, 64, 66, 68, 70, 72, 77, 80, 83-87, 90, 93 | 53 | — | 16 | 11 | 0 | 16 | 5 |
| Orthopyroxene | 9.5 | 16 | 11 | 11 | 1, 5, 10, 16, 35, 37, 55, 62, 65, 71, 94 | 28, 29, 47, 66, 70, 72, 77, 80, 84, 85, 91 | 50 | 41 | — | 9 | 5 | 0 | 0 |
| Clinopyroxene | 25.0 | 18 | 13 | 11 | 7, 21, 27, 31, 34, 41, 45, 51, 54, 69, 74, 78, 100 | 3, 8, 29, 44, 59, 67, 68, 70, 81, 83, 91 | 54 | 29 | 8 | — | 8 | 0 | 0 |
| K-feldspar | | 2.0 | | 4 | | 3, 28, 67, 81 | 0 | 0 | 25 | 75 | — | 0 | 0 |
| Cristobalite | 4.5 | 10.5 | 6 | 9 | 9, 17, 25, 30, 58, 82 | 4, 14, 40, 42, 46, 50, 64, 90, 93 | 40 | 60 | 0 | 0 | 0 | — | 0 |
| Whitlockite | | 2.5 | 2 | 1 | 20, 95 | 12 | 67 | 33 | 0 | 0 | 0 | 0 | — |
| Apatite | | 1.0 | | 2 | | 86, 87 | 0 | 100 | 0 | 0 | 0 | 0 | — |
| Ilmenite | 4.1 | | | | | | | | | | | | |
| Unidentified | | 6 | 6 | | 24, 61, 76, 88, 96, 97 | | | | | | | | |
| No peaks | | 2 | 2 | | 18, 36 | | | | | | | | |
| Mesostasis | 6.9 | | | | | | | | | | | | |
| Total | 100 | 100 | 69 | 64 | | | | | | | | | |

The results of petrographic modal analysis of a thin section (TS) of the rock are compared to the results of the modal analysis of a face of the rock obtained by Raman spectroscopy based on 100 grid points. Other results are of the identifications made by Raman spectroscopy (see Table 1). For 31 of the 100 points, signals for two (29 of the points) or three (point numbers 29 and 70) minerals were observed and data are summarized for these points. For example, of the 55 (29 single and 26 mixed) points at which plagioclase was observed, orthopyroxene was also observed at 16% of the points.

sible to distinguish with optical microscopy which particular mesostasis minerals would be illuminated by the laser beam and make the dominant contribution to the Raman signal. Also, the grain size of most mesostasis minerals is typically small, much smaller than the 30-μm thickness of the section. Thus a strong Raman scatterer at depth within the section can overwhelm a weaker scatterer at the surface. This may have been the case for K-feldspar, which is also the most abundant mineral in the mesostasis of this sample. Ilmenite is a weak Raman scatterer and did not give a signal under our operating conditions. The hematite-like spectrum (location 29) was obtained within an area of mesostasis where ilmenite was the most obvious mineral observed optically. None of the grid locations happened to fall on a zircon grain, which would have given a strong, unambiguous Raman spectrum [*Wopenka et al.*, 1996].

There are significant differences between the results obtained from the 100-point grid by Raman spectroscopy (Table 1, Raman Analysis, 100-pt Grid) and the more extensive petrographic analysis (2057 points, Table 1, Standard Analysis, Whole TS) that is based on a finer grid over the entire thin section. For example, the thin section is richer in pyroxene (31%) than indicated by either the Raman experiment (23%) or the petrographic count of those same grid locations. This difference arises from the inadequate statistical sampling of only 100 points. Such a difference would be inconsequential for most geochemical and petrological purposes. It is risky, anyway, to take the mineral proportions in one thin section, however well determined, as representative of the rock from which the thin section derived or to take the characteristics of a single rock as representative of its parent formation. The differences between the Raman results and both sets of petrographic results are thus matters of detailed classification of rock type or of point-counting statistics. They are not errors that would mislead our identification of the general rock type, which is basalt. In a lunar setting, given the preponderance of plagioclase and pyroxene, the high proportion of K-feldspar, and the grains of trace whitlockite and baddeleyite, we would readily recognize the rock as a KREEP-bearing rock, either an extrusive basalt or a relatively coarse-grained impact-melt rock.

**3.1.2. Rock fragment 15273,7039.** Because rock fragment 15273,7039 was free from interfering epoxy resin, we obtained even better results for it than for the thin section of 14161,7062. Typical spectra are shown in Figure 3. Sample 15273,7039 has a somewhat finer grain size than 14161,7062, and that plus the greater depths sampled by the laser beam gave rise to more multiphase (mixed) spectra in 15273,7039 (Table 2) than were obtained from thin section 14161,7062. Peaks from two minerals were observed in the spectra from 29 of the locations, and peaks from three minerals were observed in the spectra from two of the locations. The 100 locations analyzed on the basalt fragment yielded 131 mineral identifications. There were fewer instances of spectra having no peaks or high fluorescence in comparison to the thin section 14161,7062. Surface roughness interfered with the quality of some of the spectra, especially at two locations (18, 36) that fell on fine-grained areas that were steeply sloped along the axis of the laser beam; neither gave a peak in its spectrum. Four spectral patterns from six locations remain unidentified: locations 61 and 96 gave hematite-like spectra (the same as location 29 of 14161,7062); location 97 gave a spectrum similar to those of layered silicates; location 24 gave a spectrum with peaks near those for chromite and plagioclase; and locations 76 and 88 gave spectra similar to those of silicate glass. Spectra

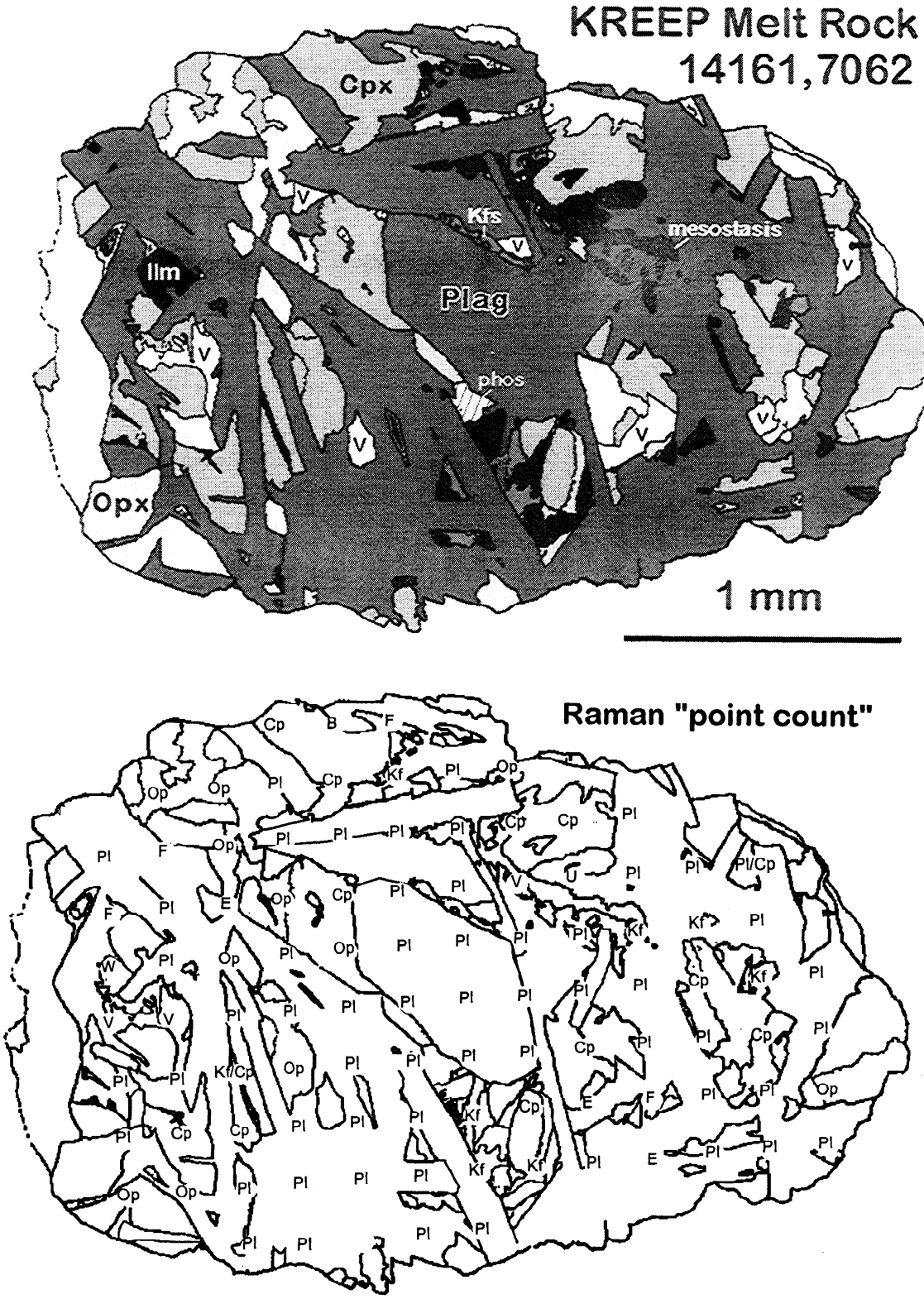


**Figure 1**. (a) Mineral map of thin section 14161,7062 KREEPy impact-melt rock fragment. Grain identifications and grain boundaries are based on reflected-light and backscattered-electron image (BEI) mosaics. The rock is rich in plagioclase and has a coarse, intergranular texture with pyroxene grains and areas of fine-grained mesostasis filling the spaces between the plagioclase mesh. In this map, the darkest mineral grains are mostly ilmenite (Ilm); slightly less dark are areas of undifferentiated mesostasis; plagioclase (Plag) is intermediate gray; K-feldspar (Kfs) is slightly lighter and occurs in areas of mesostasis, clinopyroxene (Cpx) and orthopyroxene (Opx) are lighter shades of gray and form large, composite pyroxene grains; and areas of voids (V) are white. (b). Grain boundary map of 14161,7062 showing locations and identifications of micro-Raman spot analyses. Pl, plagioclase; Cp, clinopyroxene, including pigeonite and augite; Op, orthopyroxene; Kf, K-feldspar; B, baddeleyite; W, whitlockite; E, epoxy; F, fluorescence; and V, void. The numbering scheme (see Table 1) begins with point 1 as the leftmost point in the top row, and numbering is sequential from upper left to lower right.

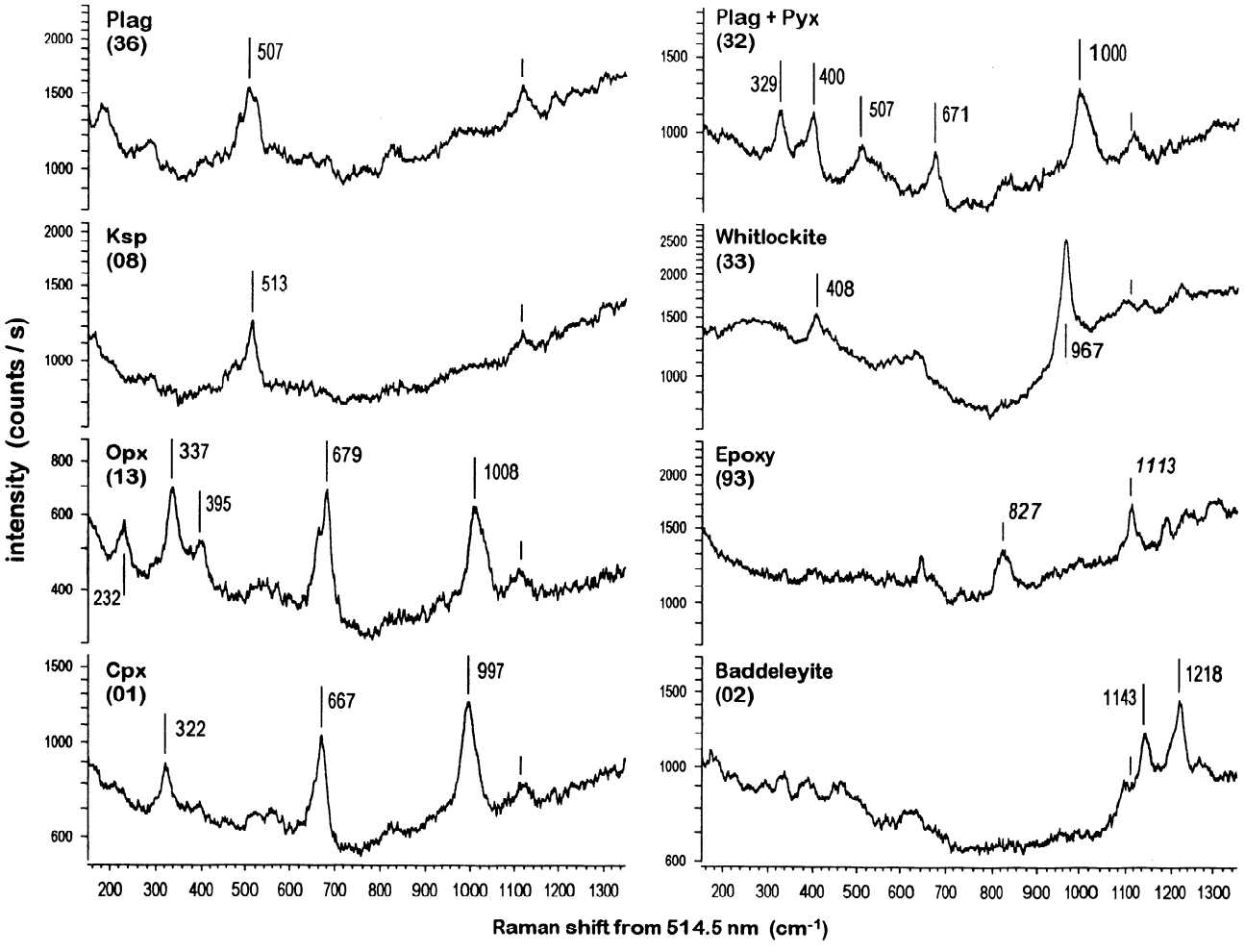


**Figure 2.** Raman spectra of grid points in sample 14161,7062 (point number in parentheses). Typical spectra of minerals occurring in the sample are shown. In each spectrum, the intensity axis is logarithmic and ranges over a factor of exactly 3, except for the whitlockite spectrum, where the axis spans a factor of 4. Positions of prominent peaks are indicated by vertical lines with wavenumber labels. The position of the epoxy peak at 1113 $cm^{-1}$ is indicated by a short vertical line in each spectrum.

similar to these could not be found during later spot analyses on the polished section of the interior of this rock fragment.

Results of the 100-point modal analysis obtained by Raman spectroscopy are compared in Table 2 to results obtained by petrographic examination of the polished section (Figure 4) made after the Raman analysis had been completed. Because the Raman analysis was done on the surface of the rock fragment but the petrographic analysis was done on an interior section, we expect some differences in mineral proportions between the two methods. The proportion of plagioclase obtained from the Raman analysis is lower than that found by petrographic analysis. The polished section reveals that plagioclase is heterogeneously distributed, so the portion of the rock surface analyzed by the Raman method may have been less plagioclase-rich than the polished section. The proportions of total pyroxene agree between the rock surface and the thin section, but the proportion of orthopyroxene is higher in the Raman analysis than in the thin section. As in the case of 14161,7062, the pyroxenes are strongly zoned, and the exact proportions of orthopyroxene and clinopyroxene are difficult to determine accurately using optical petrography, backscattered-electron imaging, or Raman analysis. The Raman analysis indicated a higher proportion of cristobalite than was found in the interior section, but cristobalite is also heterogeneously distributed. Also, the cristobalite masses are (characteristically) fractured and may have been especially susceptible to loss during the cutting and grinding stages of preparation of the polished section. In rock fragment 15273,7039, which has intergranular texture, cristobalite occurs in 50–200 μm masses that are interstitial to the mesh of plagioclase. Pyroxene and mesostasis also occupy interstitial positions (Figure 4). The sum of the proportions of the four major minerals (plagioclase, orthopyroxene, clinopyroxene, and cristobalite) is 89% for the Raman analysis and 90% for the petrographic analysis. The petrographic point count of the interior section yielded ~4% ilmenite and 7% mesostasis. This compares well with the combined 13 locations for K-feldspar, whitlockite, apatite, unknowns, and "no peaks" in the Raman analysis. Again, the identification, basalt, is evident from the mineralogy as determined by the Raman experiment and, in the lunar context, the high proportions of phosphate and cristobalite indicate an evolved lithology such as KREEP basalt.

**3.1.3. Fluorescent (photoluminescent) interference.** Photoluminescent interference (usually referred to as "fluorescent" interference in the literature of Raman spectroscopy because most such interference arises from fluorescence per se) can be a problem for mineral identification and characterization of natural

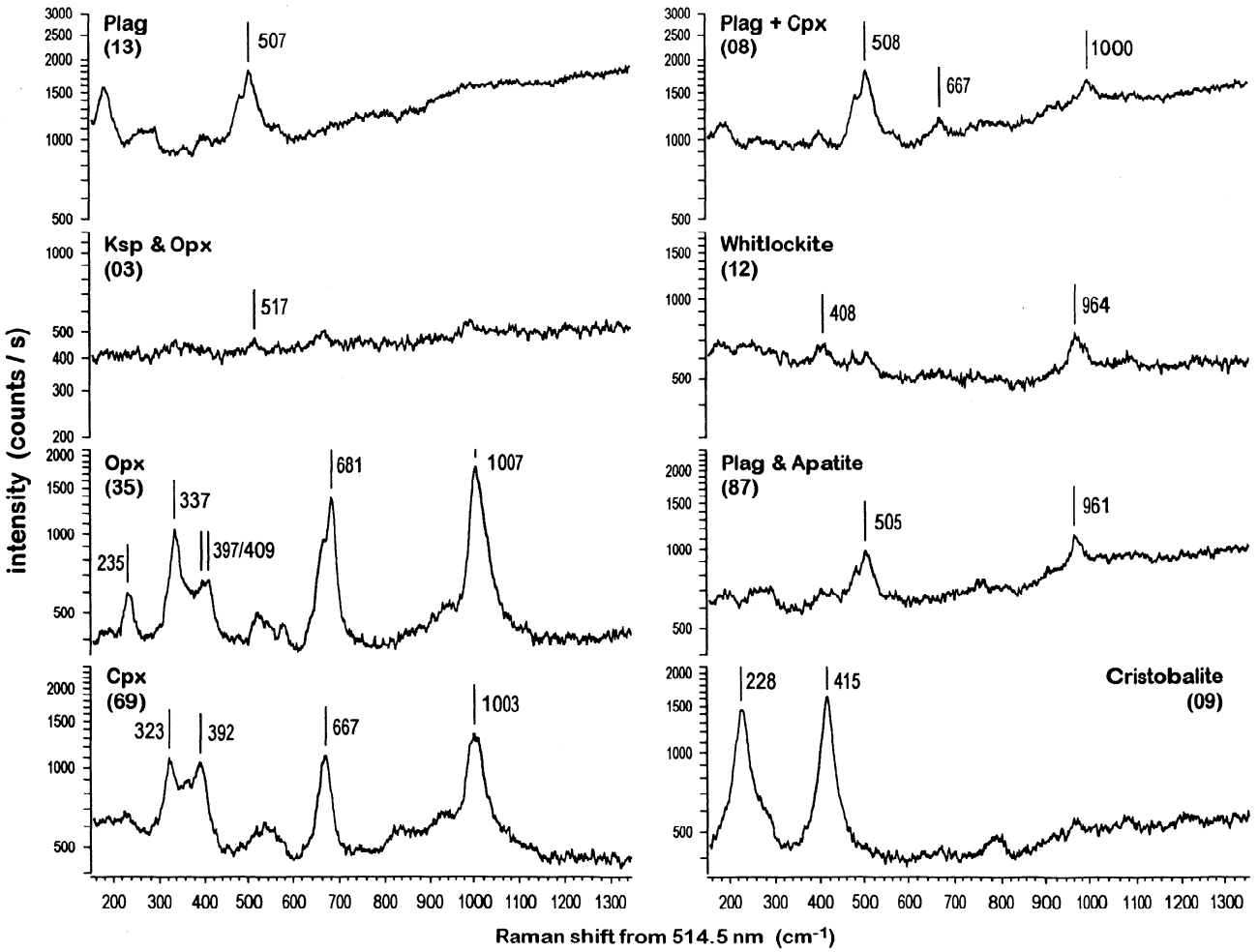


**Figure 3.** Raman spectra of grid points in sample 15273,7039 (point number in parentheses). Typical spectra of minerals occurring in the sample are shown. In each spectrum, the intensity axis is logarithmic and ranges over a factor of exactly 6. Positions of prominent peaks are indicated by vertical lines with wavenumber labels.

minerals by Raman spectroscopy. This emission sometimes overwhelms the Raman signal from the host mineral or other minerals and makes phase identification impossible. Except where strong peaks or background from epoxy resin were encountered in thin section 14161,7062, luminescence caused no such problems in our analyses of the two lunar samples. The only exception is feldspar. Raman spectra of feldspars obtained in this work commonly show high luminescence that increases strongly toward the higher wavenumber part of the spectral range (e.g., Figures 2 and 3). This broad signal did not interfere with the identification of either plagioclase or K-feldspar, as their main peaks lie in the lower wavenumber part of the spectral range. By using an exciting laser beam of longer wavelength (e.g., 683 nm [*Wang et al.*, 1997a]) the level of this interference is reduced.

Most interferences produced by luminescence in common, rock-forming minerals are caused by impurities, such as the ions of transition metals, uranium or other actinide or lanthanide elements, and organic materials (i.e., macerals, bituminous compounds, or oil) [e.g., *Rost*, 1992 ]. Most of these sources give rise to broad bands that produce high backgrounds in Raman spectra. The fluorescence spectra of lanthanide elements (rare-earth elements, REE), however, can occur as narrow peaks in the visible region of the spectrum [e.g., *Marfunin*, 1979]. The presence of some REE can be detected by means of their fluorescence spectra, and information about their valences and their positions within crystal structures can be obtained [*Marfunin*, 1979; *Jolliff et al.*, 1996]. We observed fluorescence peaks of $Er^{3+}$ [*Dieke*, 1968] in a spectrum of baddeleyite during the point count on thin section 14161,7062 (Figure 2). Such observations may also provide information about REE concentration levels in minerals [e.g., *Burruss et al.*, 1992].

### 3.2. Potential Information on Grain Size, Texture, and Mineral Associations

In addition to identifications of the major, minor, and trace minerals, information is available from Raman spectra on grain size and mineral associations of the rock. Grain size can be estimated from the frequency with which successive grid locations fall on the same mineral and from the fraction of the locations that yield multimineralic spectra. Mineral associations can be determined from the frequency of appearance of pairs of minerals in multimineralic spectra and from the frequency of appearance of pairs of minerals as adjacent grains, provided that the distance between grid locations is short enough to detect most

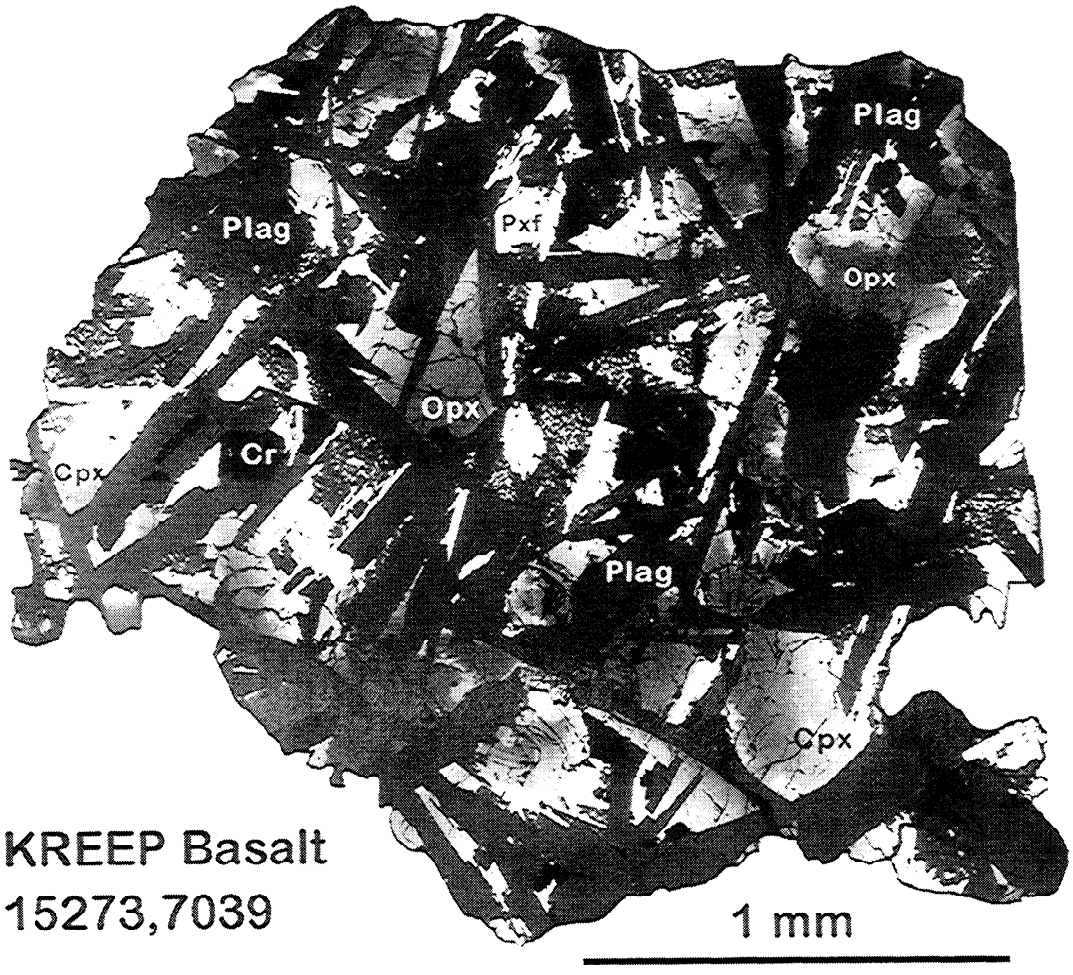


**Figure 4.** Backscattered-electron image (BEI) mosaic of polished thick section of 15273,7039 KREEP basalt fragment. In this image, minerals composed of elements of high mean atomic number are bright. The darkest phase, forming triangular to rectangular masses is cristobalite (e.g., Cr). Plagioclase, forming long, slender laths, is the most abundant mineral and is dark gray. The texture of this rock is intergranular, with pyroxene, cristobalite, and mesostasis filling the regions between the plagioclase mesh. Pyroxenes are compositionally zoned from magnesian orthopyroxene (dark, e.g., Opx) through pigeonite to Fe-augite (bright, e.g., Cpx). Some composite grains are zoned to the Fe enrichment of pyroxferroite (Mg' <5) at their rims. Several of the bright, separate grains are pyroxferroite (e.g., Pxf). The very bright, elongate grains are ilmenite. Mesostasis areas are mostly dark (glass and K-feldspar) but are speckled with high-Z phases, including ilmenite, pyroxferroite, baddeleyite, phosphates, tranquillityite, and fayalite.

neighboring mineral grains. Information on texture comes from the frequency of adjacent occurrences of minerals. Information on grain size and rock texture is supplemented by relative peak intensities of a mineral in a Raman spectrum, because relative peak intensities change with the orientation of crystal axes relative to the $\vec{E}$ of the laser beam. The applications of the Raman data to provide information on grain size, texture, and mineral associations are described below.

**3.2.1. Grain size as inferred from the frequency of occurrence of multimineralic spectra.** One method of obtaining such information is to consider the fraction of spectra that contain peaks from more than one mineral. In 14161,7062, for only two out of 89 locations did the spectra show peaks for more than one mineral. This suggests that, on average, the grains are large compared with the laser beam diameter (nominally, ~1 μm, but see below). For rock fragment 15273,7039, 31 of the spectra contained peaks from more than one mineral. This seems at first to signify an average grain size for the rock fragment that was much smaller than the average grain size observed in thin section 14161,7062, but the actual difference is not great (see Figures 1 and 4). The greater effective sampling depth for the rock fragment than for the thin section proves to be the reason for the higher fraction of multimineralic spectra from 15273,7039. The fraction of plagioclase spectra that occurred without peaks from a second mineral in 15273,7039 is 53% (Table 2), higher than the fraction for any other mineral in the sample. We might surmise that the grains of plagioclase are larger than those of the other minerals. Such a conclusion is not justified, however, unless we somehow take into account the plagioclase spectra in which contributions from two plagioclase grains might have been observed.

No single-mineral spectra were observed for K-feldspar in rock fragment 15273,7039 (Table 2); from this, we might surmise that all grains of K-feldspar are small relative to the laser

excitation volume. From examination of the polished section of the rock, we know this is the case. All locations for which whitlockite and apatite were observed produced mixed mineral spectra. Grains of the phosphate minerals tend to be small in basaltic rocks, so that observation is no surprise. We might be tempted to surmise that if phosphate spectra occurred as single mineral spectra, then the grain size of phosphates is large. This need not be true, however. Whitlockite and apatite have such high Raman scattering cross sections that peaks for other minerals excited by the laser beam can be overwhelmed by their peaks.

We may be able to obtain quantitative or semiquantitative information about typical or average grain size from the observed fraction of spectra that are multimineralic if we can properly take into account the nature of the laser excitation volume. From the observation of peaks from epoxy resin in the majority of the spectra from locations on the thin section (14161,7062), we know that the effective depth to which laser excitation provided backscattered Raman signal strong enough to be observed was >30 μm. The nominal beam size at focus is ~1 μm. In the rock sample (15273,7039), multimineralic spectra were obtained at nearly a third (31%) of the sampled locations. As a laser beam penetrates into a rock, it will encounter heterogeneities within grains and sloped boundaries between grains, not all of which have the same indices of refraction. Portions of the beam will refract and reflect in an irregular, unpredictable manner, and production and passage of Raman backscattered signal will occur over a volume whose effective area at the rock surface exceeds that of the original, focused beam. We can expect the radius of the effective area of collection of backscattered Raman signal to exceed that of the beam by perhaps several micrometers. We test this assumption with the following simple model.

We make the rough approximation that the exposed grains are square with median side length $l$. We assume that the laser spot falls randomly upon them. The surface area of each grain is $l^2$. If half of the laser spot that gave a spectrum for two minerals was on each grain, the area of the interior of the grain, where only one mineral would have been detected, is $(l-2r_b)^2$, where $r_b$ is the effective backscatter radius of the surface from which most of the Raman scattered light is collected by the objective. The effective backscatter radius substantially exceeds that of the laser beam, whose nominal diameter at focus in the present experiments was ~1 μm. Boundaries between two grains of the same mineral would not have been recognized. We assume that we would have missed mainly plagioclase-plagioclase boundaries, because plagioclase is the most abundant mineral and because pyroxene grains are zoned so that the orthopyroxene part of one grain and the clinopyroxene part of the same grain or of an adjacent grain would be counted as different grains, and other types of grains are not abundant enough to bound each other commonly if randomly distributed. We estimate that we would have missed approximately $(0.42)^2/(0.42 \times 0.58) \times 31$, or 22 plagioclase-plagioclase boundaries. The estimated total number of observed boundaries is thus 53 out of the 100 sampling locations. The median grain size of the principal mineral, plagioclase, in rock 15273,7039, based on examination of the polished section, is ~120 μm. Based on this value of $l$, $[l^2 - (l-2r)^2]/l^2 \sim 0.53$, so $r_b$ ~ 19 μm. Whether we can calibrate a series of rocks and obtain a consistent and useful value for the parameter $r_b$, the effective scattering radius, which we could use to determine approximate median grain size, remains to be determined. The results from thin section 14161,7062 cannot be used for this purpose because the laser beam penetrated through the rock.

**3.2.2. Mineral associations inferred from statistics of adjacent mineral grains and the frequency of mulitmineralic spectra.** If grid locations for a mineral occur adjacent to grid locations for the same mineral or adjacent to another specific mineral more frequently than expected for random occurrence, then we may suspect one or more of the following (some of which may be equivalent in a given case): In the case of same-mineral pairs, grains of that mineral are large relative to the distance between locations, or grains of that mineral are heterogeneously distributed within the rock. In the case of different-mineral pairs, the minerals may be petrogenetically associated with each other. For simplicity in the following discussion, we treat the locations in consecutive order as if they had been taken as a single line of data, and thus we ignore the two-dimensional-grid aspect of the experiment. More sophisticated data treatments could be used to search for clustering in a grid experiment, but the approach used here is applicable to data taken along a linear traverse.

The frequency of occurrences of successive locations with the same mineral will depend on both grain size and shape. The appendix provides one model, as an example, of the distribution of traverse distances and the average traverse distance expected for randomly oriented rectangular grains (in two dimensions). This model provides a rough idea of how frequently we might expect adjacent locations to land on a single grain of lath-shaped plagioclase, the most common and coarsest mineral in these samples. The principal result is that for random orientation, we would expect only a small fraction of plagioclase laths to be traversed approximately parallel to their long axes. Thus, in a linear traverse, we would only occasionally expect a location to fall on the same plagioclase grain as the previous location, given our >200 μm distance between locations. The same rationale is used in all the following statistical calculations: (1) calculate the probability $P$ of a certain situation occurring, (2) calculate $N$, the number of expected occurrences ($100P$), and (3) using Poisson statistics, calculate the probability of obtaining $M$ occurrences ($M$ usually >$N$).

In the Raman point count of thin section 14161,7062, plagioclase was identified at 57 of the 100 locations (Table 1, Single plus Mixed). If for a given plagioclase grain at location $n$ the identity of location $n$+1 is independent of the identity of location $n$, then the probability is 0.56 that location $n$+1 is also plagioclase, and we would expect the number of occurrences of both locations $n$ and $n$+1 being plagioclase to be 32 (=57×0.56). The number of occurrences must fall within the limits of 56 (all plagioclases clustered together) and 14 (all nonplagioclases followed by a plagioclase), but from Poisson statistics, we would expect that 90% of the time the number of occurrences would lie in the range 23–41. The observed number of occurrences of both locations $n$ and $n$+1 being plagioclase is 34, not significantly different from the expected value of 32. Similar results are obtained for the other minerals. Thus we can reasonably conclude that (1) the occurrence of the same mineral twice in a row does not happen more frequently than we would expect if the identity at a given location is independent of that of an adjacent location and (2) there is consequently no evidence that plagioclase or other mineral grains are large compared to the distance between grid locations. These conclusions are consistent with the observed grain sizes and morphology of the sample. In practice, accurate interpretation of information of this type in terms of grain size will probably depend on analogy with grain morphology in terrestrial rocks of similar lithology.

In thin section 14161,7062, K-feldspar was identified at eight locations and clinopyroxene at 12 (Table 1, Single and Mixed).

The probability that a given location adjacent to a K-feldspar is clinopyroxene is 0.12, so with 16 adjacent locations we would expect about 16×0.12 = 2 K-feldspar–clinopyroxene pairs. The observed number of pairs is four, and the probability of obtaining four or more is only 13% if the probability of K-feldspar or clinopyroxene occurring at a given location is related only to the relative abundance of the mineral in the thin section. The analysis suggests weakly that K-feldspar might be associated with clinopyroxene in the crystallization sequence. This is possible, because the mesostasis consists mainly of clinopyroxene (Fe-augite and pyroxferroite). A similar enhancement might be expected for K-feldspar-K-feldspar pairs; two were observed, although the probability of obtaining two or more is only 11%.

We also consider adjacent grain identities for rock fragment 15273,7039 (Table 2). Again, the data were treated in consecutive order as if there had been a single traverse across a larger rock, and again, there is no evidence from the Raman traverses for a nonrandom distribution of plagioclase or for a large size of patches of mesostasis. The distance between grid locations was ~330 μm. We observed an improbably high K-feldspar-clinopyroxene adjacent-grain frequency in thin section 14161,7062, and similarly, in rock fragment 15273,7039, we observed six occurrences of K-feldspar adjoining clinopyroxene, which is even more improbable (1.4% of obtaining six or more) if we assume that the distribution of K-feldspar grains is unrelated to that of clinopyroxene. In contrast to the results for 14161,7062, there are no occurrences of K-feldspar–K-feldspar pairs in 15273,7039, however, and that is the result we would expect if the minor K-feldspar were distributed randomly in the rock (the probability is only 11% of obtaining 1 or more pairs). The observed high frequency of K-feldspar-clinopyroxene associations in both samples is puzzling from a statistical point of view. In both samples, K-feldspar and clinopyroxene are the principal minerals in the mesostasis, and all of the K-feldspar is in mesostasis, but not all of the clinopyroxene is in the mesostasis. There is a petrographically observable, imperfect association in each rock between clinopyroxene and K-feldspar, but we would not expect to observe it in the statistics of adjacent grains because the sizes of most clinopyroxene grains and patches of mesostasis are smaller than the distance between grid locations. We would expect to observe such an association if the clinopyroxene grains and patches of mesostasis were grouped and not randomly placed.

In 15273,7039, we see that of the 15 locations at which cristobalite was identified, nine (60%) occurred in mixed mineral spectra (Table 2) and that the accompanying mineral in all nine cases is plagioclase. Given that 50% of the rock is plagioclase, we would expect only four to five occurrences in which plagioclase was the mineral that accompanied cristobalite, and the probability is only 4% that the number of occurrences would be nine or more, as was observed, if the distribution of cristobalite were unrelated to that of any other mineral. Thus we can reasonably surmise that cristobalite is texturally associated with plagioclase in the rock. In general, adjacent occurrences of closely associated minerals will occur more frequently than random only if the spacing between grid locations is of the order of the average traverse distance across mineral grains or shorter. If the grid locations are too far apart, associations would be missed. If the spacings are intermediate, spurious associations might be suspected because the grain under the next point would almost never be the adjacent, related mineral. It will thus be essential to use general petrological information to interpret the possible significance of any associations indicated by adjacent-grain statistics.

**3.2.3. Grain size and rock texture based on the variability of peak positions and intensity ratios.** In cases of adjacent grid locations and strings of locations for a particular, single mineral, we may want to know whether successive spectral measurements have fallen on the same grain of that mineral. We can in principle support or rule out such a suspicion on the basis of differences in peak positions or in relative intensities between pairs of peaks, as described below.

Peak positions appear to be of limited use for determining whether spectra of a given mineral taken at adjacent grid locations are part of a single grain. Positions of the principal pyroxene peaks and overall spectral patterns appear to depend on pyroxene crystal structure (orthorhombic and monoclinic pyroxenes, and triclinic pyroxenoid) [*Delé-Dubois et al.*, 1981; *Wang et al.*, 1995]. Pyroxene grains in the samples tested are strongly zoned, in some cases from orthopyroxene to clinopyroxene, so that a change in structure does not necessarily indicate a change in grain. We also find for these pyroxenes that peak positions depend systematically on composition (proportions of $Ca^{2+}$, $Mg^{2+}$, and $Fe^{2+}$) [*Wang et al.*, 1997b]. This dependence could prove useful for constraining chemical compositions, but it is complex, and its description and explanation are beyond the scope of this paper. Compositional zoning within crystals reduces the chance that a difference in Raman peak positions between grid locations would indicate that two different pyroxene grains had been sensed. For plagioclase, we have found no dependence of peak positions on chemical compositions over the range of anorthite contents typical of lunar rocks; peak positions were found to be at most slightly variable, with standard deviations of 2–3 $cm^{-1}$. We have not yet examined plagioclase more albitic than $An_{50}$. The change over the compositional range from anorthite to albite appears to be small, however [*Sharma et al.*, 1983]. The Raman spectrum of plagioclase is distinguishable from that of orthoclase.

Peak intensities of a given mineral taken under the conditions of these experiments vary substantially. For example, all spectra of 15273,7039 were taken with constant laser power impinging on the sample surface and over a constant integration time. Nevertheless, peak heights (above background) varied substantially for a given mineral. Standard deviations about mean peak heights are typically ±40–60%. Ratios of maximum to minimum peak heights vary by factors of ~3 to 8. Factors affecting Raman scattering intensity were discussed in the introduction and are not reviewed here.

Not only peak intensities but peak intensity ratios vary substantially from spectrum to spectrum of the same mineral. Reasons for this variability are still under study; here, we discuss one of the principal causes, differences in grain orientation. A large difference in peak intensity ratios between spectra of the same mineral taken at adjacent locations is evidence for separate crystals of that mineral, oriented differently relative to the direction of polarization of the laser beam.

To demonstrate effects of grain orientation, with minimum effects of surface roughness, we obtained multiple spectra on each of several grains in the thin section of 14161,7062 and the polished section of 15273,7039 by rotating each grain in the axis of the laser beam. We determined relative peak intensities under constant conditions for four grains of plagioclase in the thin section of 14161,7062 and for one grain of plagioclase and three grains of pyroxene in the polished section of 15273,7039. In

these experiments, the position of the laser on each grain was fixed; the grain rotated as the microscope stage was turned. The purpose of the experiments was to demonstrate potential effects of grain orientation on spectra from a particular mineral under field conditions, where spectra might be taken from several grains with different orientations relative to the polarization of the laser beam, and not to determine the maximum possible effect or to attribute a particular peak to a specific vibrational mode.

The results for one of the grains of orthopyroxene (in 15273,7039), determined at three orientations, one with cleavages aligned along $\vec{E}$ of the laser beam polarization, one with cleavages aligned perpendicular to $\vec{E}$, and one with cleavages aligned 45° to the $\vec{E}$, are shown in Figure 5. Rotating the microscope stage through 90° changed even the qualitative appearance of the spectra. The effect occurs because the laser beam is polarized and couples with each different vibrational transition with a strength that is described by a polarizability tensor and depends on the orientations of the crystal axes relative to the $\vec{E}$ of the beam [e.g., *Long*, 1977]. The main peaks were fit to determine their positions and heights (Grams/32 curve-fitting program, with Gaussian-Lorentzian mixed peak shape, linear baseline, and a free constraint iteration to convergence of all parameters, including the peak position, height, width, mixing percentage for each peak, and slope and intersection for baseline). For the main peaks, the variations in peak position were ≤1 $cm^{-1}$. The variations in peak heights were <2× in most cases, significantly smaller than the overall variation (typically, ~3 to ~7×) for orthopyroxenes in the rock, where the surface is rough.

Similar rotation experiments were done on grains of plagioclase; results for two of these grains (from 14161,7062) at two orientations each are shown as examples in Figure 6. Rotation changes the relative peak intensities in each grain. The spectra for the different grains differ qualitatively in appearance from each other beyond the changes caused by rotation, however. This is because the principal axis of each grain is oriented at a different angle relative to the plane of the thin section. The spectral features of the four grains are so different that some peaks readily observed in one or more grains are small or absent in another grain (e.g., the 287 $cm^{-1}$ peak is essentially absent from the spectrum for grain 1 and the 189 $cm^{-1}$ peak is overcome by a 200 $cm^{-1}$ peak in the spectrum of grain 4) (not shown). The 187 $cm^{-1}$ peak is relatively high compared with the 509 $cm^{-1}$ peak in the spectrum of grain 2, but the 509 $cm^{-1}$ peak is much stronger than any lower energy peak in grain 4. The 410/509, 491/509, and the 491/563 peak intensity ratios were unchanged as a consequence of rotation in all four plagioclase grains.

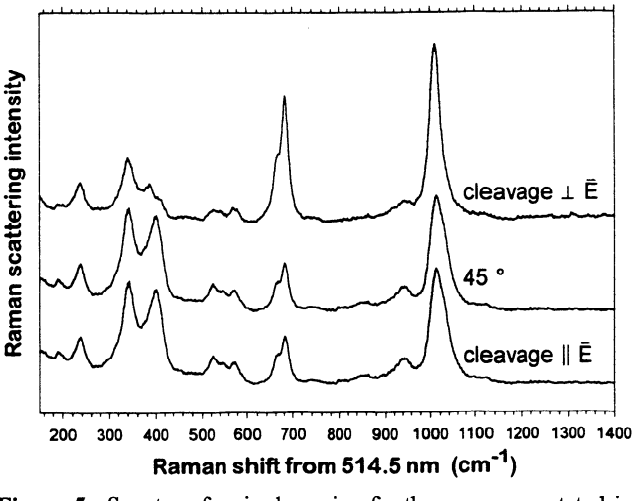


**Figure 5.** Spectra of a single grain of orthopyroxene, rotated in the plane of the polished section of 15273,7039 through 90° from alignment along the $\vec{E}$ of the laser beam. Note the changes in relative peak heights and the change in spectral pattern caused by the rotation. Spectra are offset along the ordinate (Raman scattering intensity).

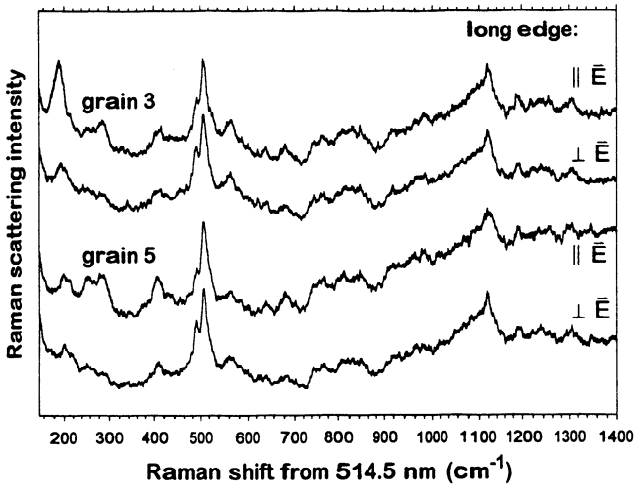


**Figure 6.** Spectra of two plagioclase grains in the thin section of 14161,7062, rotated from their long edges parallel to $\vec{E}$ to perpendicular to $\vec{E}$. Note the change in spectral pattern and relative peak heights on rotation for each grain, and note the difference in spectral patterns between the two grains, which arises because of different grain orientations relative to the axis of the laser beam. As in Figure 5, spectra are offset from each other along the ordinate.

We now consider pairs of spectra taken at adjacent locations in thin section 14161,7062, for which grid locations falling on the same grain of plagioclase are known. During the point-counting experiments, there was no change in orientation of the grains relative to the $\vec{E}$ of the laser beam. The spread in peak intensity ratios among the spectra for each of the single grains is substantially less than that for the entire suite of plagioclase grains considered as a group. This confirms that relatively small changes in peak height ratios for adjacent Raman locations can be used as one test of whether adjacent locations may have been on the same grain or on grains that may be similarly aligned as a consequence of rock texture (or by accident). Similarly, for orthopyroxene, same-grain spectra vary less in peak intensity ratios than those for the suite of orthopyroxene grains treated as a group. Based on the sparse data, a similar claim cannot be made for clinopyroxenes, but that is reasonable, given the greater extent of compositional zoning in that mineral.

Applying these results to the analysis of spectra from 15273, 7039, we find no evidence for successive locations on single mineral grains. This result is not surprising, as the Raman spectra were taken ~330 μm apart, substantially farther apart than the typical dimensions of the minerals except the longest plagioclase laths. As seen from Figure A2, only a small fraction of plagioclase laths 50 μm in width would be oriented with their long dimensions parallel or nearly so to the path of a traverse, so only seldom would two successive plagioclase-only locations fall on the same grain.

## 4. Conclusions

This work confirms the potential value of Raman spectroscopy for silicate mineral analysis for use on a planetary surface. It shows how the method can be used to provide information on all three aspects of mineralogical analysis: mineral identification, mineral composition, and mineral proportions. The identification comes from peak positions, which are nonoverlapping for the major and most minor minerals. Information on chemical compositions (mineral end members) can be obtained from peak positions for olivine and possibly pyroxene. Information on pyroxene structural type can be obtained from spectral patterns and peak positions, as well. Quantification of the mineral proportions in a rock can be obtained by point counting, i.e., the fraction of spectra that contain a peak for each mineral, without concern about peak intensities.

Both the Raman point count and the petrographic point count identify minerals under the grid locations precisely and accurately. They did not observe the same mineral at every location, however. Raman spectroscopy provides correct information on the minerals excited sufficiently by the laser beam to give Raman peaks, but the Raman signal comes from a volume around and beneath the location where the laser impinges on the sample. Petrographic examination also gives correct information, but only about the surface phase in reflected light petrography or on electron-backscatter images, which were used for most of the work reported here. Sometimes a Raman spectrum indicated a mineral that was obscured from petrographic identification.

It is clear from the experiments described above that quantifying proportions of minerals on the basis of their Raman peak intensities would be highly imprecise at best. Uncontrollable parameters in a planetary surface Raman analysis include position of laser beam focus, mineral transparency, mineral thickness, effective depth of penetration of the beam into the sample, surface angle of the target surface to the beam (reflection rather than transmission of the incident beam), grain boundaries and grain scattering of incident and Raman-scattered radiation (more severe in finer-grained rocks), and crystal orientation. Thus there is no simple relationship between peak height and mineral proportion. It is doubtful that even extensive calibration would enable quantification on such a basis. Effects of the above parameters are nevertheless worth further study and should be better understood in interpreting spectra from a planetary surface. Our study of Raman point counting suggests we can successfully circumvent them, however, at least in the common, straightforward case of a rock yielding good spectra from most analyzed locations.

We can obtain information about grain sizes and mineral associations by analysis of the frequency of occurrence of multimineralic spectra and the statistics of adjacent grain identities. We obtain further information on rock textures by examining peak height ratios between spectra of the same mineral taken at adjacent Raman locations. For rocks as fine-grained as the KREEP basalts examined here, however, the adjacent locations need to be taken closer together if single grains are to be detected.

## Appendix: Estimated Distribution of Traverse Distances as a Function of Angle Across Randomly Oriented Rectangular Grains

Consider rectangular grains with length of $2a$ and width of $2b$ that are randomly oriented in the plane of a thin section or rock surface (Figure A1). The average distance $D$ across such grains

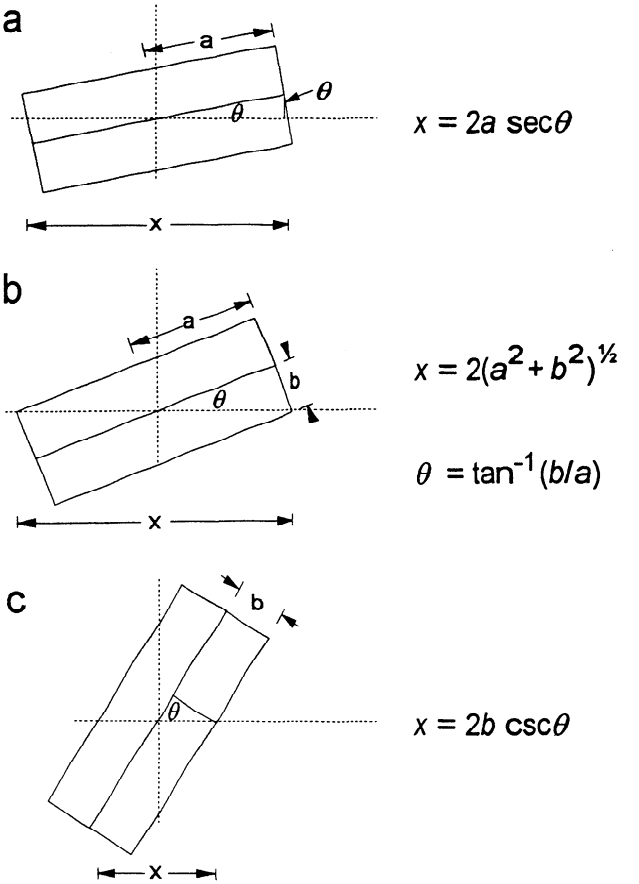


**Figure A1.** Schematic diagram of a rectangular grain and equations for determining the traverse distance along the $X$ axis as a function of the angle $\Theta$ between the $X$ axis and the long axis of the crystal.

that would be encountered on a linear traverse can be calculated as the integral of distances from $\Theta = 0°$ to $90°$ divided by the integral of $d\Theta$ between those same limits, where $\Theta$ is the angle of the long axis of the crystal relative to the direction of the traverse (taken to be along the $X$ axis). The distance as a function of $\Theta$ is dependent mainly on grain length (equation (1)), from $\Theta = 0$ to $\Theta$, the angle corresponding to alignment of the diagonal along the $X$ axis (equation (2), Figures A1a and A1b). For higher angles it is dependent mainly on grain width, and is given by equation (3) (Figure A1c):

$$D_1 = 2a \sec(\Theta) \qquad (0 \text{ to } \Theta_{diag}) \qquad (1)$$

$$\Theta_{diag} = \tan^{-1}(b/a) \qquad (2)$$

$$D_2 = 2b \csc(\Theta) \qquad (\Theta_{diag} \text{ to } \pi/2) \qquad (3)$$

The average traverse distance, is given by

$$D = (4a/\pi)\ln[\pi/4 + (1/2)\tan^{-1}(b/a)] - (4b/\pi)\ln\{\tan[(1/2)\tan^{-1}(b/a)]\} \qquad (4)$$

Figure A2a shows the distance in μm traversed as a function of $\Theta$ for crystals of several lengths and two widths. The distance rises with increasing $\Theta$ from the crystal length ($2a$) to the diagonal length, then decreases with increasing $\Theta$ to the crystal width. The initial increase is not obvious on the graph because the diagonal lengths for long, thin laths is not much longer than the length of the crystal; it shows up most strongly for the more

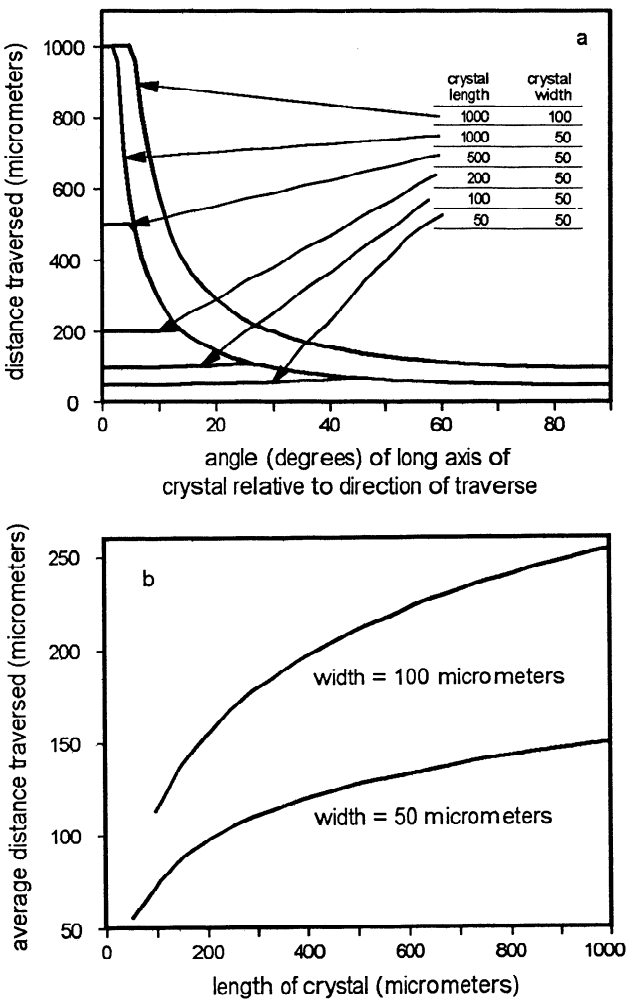


**Figure A2.** (a) The distance traversed along the $X$ axis is shown as a function of the angle $\Theta$ for rectangular grains of several aspects and two widths. (b) The average distance traversed for crystals of two widths oriented randomly with respect to the $X$ axis are shown as a function of crystal length.

nearly square crystals (e.g., 50 μm × 50 μm). Over only a short range of angles (0 to ~6° for a width of 50 μm and 0 - ~12° for a width of 100 μm) does a traverse cross as much as half the length of the crystal. Thus most characteristic distances are short relative to the length of the long axis of the crystal if angles of orientation are random relative to the direction of the traverse. The average traverse distance for such randomly oriented crystals is shown as a function of crystal length for crystals of two widths, 50 and 100 μm in Figure A2b.

**Acknowledgments.** We thank J. Pasteris for the use of her Raman spectrometer, and we thank her and B. Wopenka for helpful discussions. We appreciate reviews of the manuscript by R. Morris and T. Wdowiak. This work was supported in part by NASA under grants NAGW 5207 and 3343.

## References

Burruss, R. C., T. G. Ging, R. G. Eppinger, and I. M. Samson, Laser-excited fluorescence of rare earth elements in fluorite: Initial observations with a laser Raman microprobe, *Geochim et Cosmochim. Acta, 56*, 2713 2723, 1992.

Delé-Dubois, M. L., P. Dhamelincourt, and H. J. Schubnel, Etude par spectroscopie Raman d'inclusions dan les diamonts, saphirs et émeraudes, *Rev. Fr. Gemmol., 64*, 13-16, 1981.

Dieke, G. H., *Spectra and Energy Levels of Rare Earth Ions in Crystals*, Wiley-Interscience, New York, 1968.

Dyar, M. D., A. Treiman, P. Beauchamp, D. Blake, D. Blaney, S. S. Kim, G. Klingelhöfer, G. Mehall, R. Morris, Z. Ninkov, A. Sprague, M. Zolensky, and C. Pieters, Mineralogy, in *Planetary Surface Instruments Workshop*, edited by C. Meyer, A. H. Trieman, and T. Kostiuk, *LPI Tech. Rep. 95-05*, pp. 65-84, Lunar and Planet. Inst., Houston, Tex., 1996.

Estep, P. A., J. J. Kovach, P. Waldstein, and C. Karr Jr., Infrared and Raman spectroscopic studies of structural variations in minerals from Apollo 11, 12, 14, and 15 samples, *Proc. Lunar Sci. Conf., 3rd*, 3047-3067, 1972.

Israel, E. J., R. E. Arvidson, A. Wang, and B. L. Jolliff, New approaches to the in-situ study of Martian surface mineralogy (abstract), *Lunar Planet. Sci., 27*, 583-584, 1996.

Israel, E. J., R. E. Arvidson, A. Wang, J. Pasteris, and B. L. Jolliff, Laser Raman spectroscopic measurements of a desert-varnished basalt and implications for in-situ analysis of martian rocks (abstract), *Lunar Planet. Sci., 28*, 625-626, 1997.

Jolliff, B. L., R. L. Korotev, and L. A. Haskin, Geochemistry of 2-4-mm particles from Apollo 14 soil (14161) and implications regarding igneous components and soil-forming processes, *Proc. Lunar Planet. Sci. Conf., 21st*, 193-219, 1991.

Jolliff, B. L., J. J. Freeman, and B. Wopenka, Structural comparison of lunar, terrestrial, and synthetic whitlockite using laser Raman microprobe spectroscopy (abstract), *Lunar Planet. Sci., 27*, 613-614, 1996.

Kerridge, J., D. DesMarais, R. K. Khanna, R. Mancinelli, G. McDonald, F. Radicatti di Brozollo, and T. Wdowiak, Carbon-based compounds and exobiology, in *Planetary Surface Instruments Workshop*, edited by C. Meyer, A. H. Trieman, and T. Kostiuk, *LPI Tech. Rep. 95-05*, pp. 85-96, Lunar and Planet. Inst., Houston, Tex., 1996.

Korotev, R. L., Mixing levels, the Apennine Front soil component, and compositional trends in the Apollo 15 soils, *Proc. Lunar Planet. Sci. Conf., 17th, Part 2, J. Geophys. Res., 92*, suppl., E411-E431, 1987.

Korotev, R. L., L. A. Haskin, and B. L. Jolliff, A simulated geochemical rover mission to the Taurus-Littrow valley of the Moon, *J. Geophys. Res., 100*, 14,403-14,420, 1995.

Long, D. A., *Raman Spectroscopy*, McGraw-Hill, New York, 1977.

Marfunin, A. S., *Spectroscopy, Luminescence and Radiation Centers in Minerals*, 352 pp., Springer-Verlag, New York, 1979.

Meyer, C., A. H. Trieman, and T. Kostiuk (Eds.), *Planetary Surface Instruments Workshop, LPI Tech. Rep. 95-05*, 115 pp., Lunar and Planet. Inst., Houston, Tex., 1996.

Morris, R. V., R. Score, C. Dardano, and G. Heiken, *Handbook of Lunar Soils I, Planet. Mater. Br. Publ. 67, JSC 19069*, 216 pp., Johnson Space Center, Houston, Tex., 1983.

Rost, F. W. D., *Fluorescent Microscopy*, Cambridge Univ. Press, New York, 1992.

Sharma, S. K., B. Simons, and H. S. Yoder Jr., Raman study of anorthite, calcium Tschermak pyroxene and gehlenite in crystalline and glassy states, *Am. Mineral., 68*, 1113-1125, 1983.

Wang, A., B. L. Jolliff, and L. A. Haskin, Raman spectroscopy as a method for mineral identification on lunar robotic exploration missions. *J. Geophys. Res., 100*, 21,189-21,199, 1995.

Wang, A., E. Cortez, and L. A. Haskin, A Raman spectroscopic sensor for on-surface planetary remote sensing (abstract), *Lunar Planet. Sci., 28*, 1489-1490, 1997a.

Wang, A., B. L. Jolliff, K. M. Viskupic, and L. A. Haskin, Raman spectroscopic characterization of different types of pyroxene (abstract), *Lunar Planet. Sci., 28*, 1491-1492, 1997b.

Wdowiak, T. J., D. G. Agresti, and S. B. Mirov, A laser Raman spectrometer system suitable for incorporation into lander spacecraft (abstract), *Lunar Planet. Sci., 26*, 1473-1474, 1995.

Wopenka, B., B. L. Jolliff, E. Zinner, and D. K. Kremser, Trace element zoning and incipient metamictization in a lunar zircon: Application of three microprobe techniques, *Am. Mineral.*, 81, 902–912, 1996.

L. A. Haskin, B. L. Jolliff, R. L. Korotev, K. M. Rockow, K. M. Viskupic, and A. Wang, Department of Earth and Planetary Sciences, Washington University, One Brookings Drive, St. Louis, MO 63130. (e-mail: lah@levee.wustl.edu)

(Received January 28, 1997; revised May 21, 1997; accepted June 9, 1997.)